Micro-Mold Design Controls the 3D Morphological Evolution of Self-Assembling Multicellular Microtissues

Alexander A. Svoronos, BS,[1,2,*] Nalin Tejavibulya, BS,[1,2,*] Jacquelyn Y. Schell, PhD,[1,2]
Vivek B. Shenoy, PhD,[3] and Jeffrey R. Morgan, PhD[1,2]

When seeded into nonadhesive micro-molds, cells self-assemble three-dimensional (3D) multicellular microtissues via the action of cytoskeletal-mediated contraction and cell–cell adhesion. The size and shape of the tissue is a function of the cell type and the size, shape, and obstacles of the micro-mold. In this article, we used human fibroblasts to investigate some of the elements of mold design and how they can be used to guide the morphological changes that occur as a 3D tissue self-organizes. In a loop-ended dogbone mold with two nonadhesive posts, fibroblasts formed a self-constrained tissue whose tension induced morphological changes that ultimately caused the tissue to thin and rupture. Increasing the width of the dogbone's connecting rod increased the stability, whereas increasing its length decreased the stability. Mapping the rupture points showed that the balance of cell volume between the toroid and connecting rod regions of the dogbone tissue controlled the point of rupture. When cells were treated with transforming growth factor-β1, dogbones ruptured sooner due to increased cell contraction. In mold designs to form tissues with more complex shapes such as three interconnected toroids or a honeycomb, obstacle design controlled tension and tissue morphology. When the vertical posts were changed to cones, they became tension modulators that dictated when and where tension was released in a large self-organizing tissue. By understanding how elements of mold design control morphology, we can produce better models to study organogenesis, examine 3D cell mechanics, and fabricate building parts for tissue engineering.

Introduction

Scaffold-free methods for forming three-dimensional (3D) tissues are growing in importance in tissue engineering. Without a scaffold, cells will aggregate and self-assemble functional 3D microtissues.[1] These small tissues have high cell densities akin to that of native organs. Cell-to-cell interactions such as cell–cell communication are maximized, and overall differentiated function is enhanced.[2–8] Self-assembly is driven by the concerted actions of various surface adhesion molecules (e.g., cadherins, connexons) along with cytoskeletal-mediated contraction, and it is thought to mimic the aspects of embryogenesis, morphogenesis, and organogenesis.[9–14] Different cell types vary with regard to their rate and extent of self-assembly.[13,15] Movement of individual cells occurs as a loose layer of cells aggregate and form a 3D multicellular tissue with substantial x, y, and z dimensions. In addition to climbing over one another, cell movements can be quite specific, as evidenced by the self-sorting that can occur when a mixture of two cell types self-assemble.[1,11,12] With some mixtures, one cell type will form the inner core of the spheroid, whereas the other cell type forms the outer coating. Self-sorting occurs concurrently with the overall self-assembly process.[16]

In addition to the spheroid geometry, we have shown that cells can self-assemble into microtissues with complex shapes, such as rods, toroids, and honeycombs.[15,17–19] In this process, known as directed self-assembly, cells are seeded into a micro-mold made from a nonadhesive hydrogel that does not interfere with the cell-to-cell interactions that drive self-assembly. The mold does, however, contain nonadhesive obstacles (e.g., posts) that direct the self-organizing tissue toward specific outcomes in terms of size and shape. For example, a large ~2 cm honeycomb tissue was self-assembled in a mold with posts arranged in eight concentric circles.[19] In addition to the movements of cells, there are significant tissue movements or morphological changes during directed self-assembly. These movements, driven by cell-generated tension, occur in response to the size, shape, and placement of the obstacles in the mold.

[1]Department of Molecular Pharmacology, Physiology and Biotechnology, [2]Center for Biomedical Engineering, Brown University, Providence, Rhode Island.
[3]Department of Bioengineering, University of Pennsylvania, Philadelphia, Pennsylvania.
*Both authors contributed equally to this work.

Here, we show how micro-mold design elements can control the morphological evolution of a self-organizing tissue. Human fibroblasts, a rapidly self-assembling cell type, were used to determine how mold design influences tissue self-organization. By measuring the kinetics of morphological changes at various locations, we found three distinct phases of self-organization. Unlike other cell types, fibroblasts generate enough tension to cause tissue rupture in constrained tissues, thus we used these cells to determine tissue stability and the locations of rupture as a function of tissue length, width, and growth factor treatment. Finally, we modified the design of the obstacles and demonstrated their use as tension modulators that control tissue morphology and release tension at desired positions in complex-shaped tissues.

Materials and Methods

Nonadhesive micro-molds

Wax molds were designed using SolidWorks (Solid Works Corporation, Concord, MA) and produced with a Thermo-Jet1 rapid prototyping machine (3D Systems Corporation, Valencia, CA). Mold fidelity was qualitatively assessed using a SteREO Discovery.V12 dissecting microscope (Carl Zeiss MicroImaging GmbH, Göttingen, Germany). Loop-ended dogbone recesses were 1.5 mm deep and consisted of tori with inner diameters of 800 μm and outer diameters of 2.4 mm connected by troughs of width 300, 400, 600, or 800 μm. Dogbone length, measured from the center of one toroid to the other, was 6, 9, or 12 mm. Rod-shaped troughs were included between dogbone recesses to eliminate dead space and facilitate uniform cell seeding.

The mold for forming microtissues in the shape of three interconnected toroids (three ring) had three obstacles, posts (P) or cones (C) (65° slope), situated in a straight line. The mold for forming honeycombs had a total of 19 obstacles (posts or cones) arranged in two orbitals around a single obstacle in the center. The posts and cones for the three-ring and honeycomb molds were 800 μm in height and 800 μm in base diameter, and all were surrounded by a continuous trough 400 μm wide.

Polydimethylsiloxane (PDMS) (Sylguard 184; Dow Corning, Midland, MI) molds were cast directly from the wax dogbone molds. The molds were subsequently washed and sterilized. A 2% molten agarose solution (0.9% saline) was cast into each PDMS mold. Agarose gels were then separated from the molds and equilibrated with the tissue culture medium.

Three-ring tissues and honeycomb tissues were formed in nonadhesive polyacrylamide molds. Polyacrylamide gels (13%) were cast directly from wax prototypes. Polymerized gels were removed from the wax and rinsed three times over several hours with the serum-free medium. Twenty-four hours before seeding, gels were rinsed and incubated in the serum-containing medium.

Production of self-assembled microtissues

Normal human fibroblasts (NHF) derived from neonatal foreskins were expanded in high-glucose Dulbecco's modified Eagle's medium supplemented with 10% fetal bovine serum and 1% penicillin/streptomycin and maintained at 37°C, 10% CO_2, and used between passages 3 and 12. For

fluorescent imaging, cells were labeled with CellTracker™ Green CMFDA (Invitrogen, Eugene, Oregon) according to the manufacturer's protocol.

Seeding of the gels has been described elsewhere.[17,18] Briefly, excess medium was aspirated from the wells, and a small volume of a single-cell suspension was pipetted into the main recess of each gel. The 6, 9, and 12 mm dogbone molds containing eight dogbone-shaped recesses were seeded with 2.1×10^6, 2.8×10^6, and 3.75×10^6 cells, respectively, corresponding to 18,000 cells per mm^2 of mold recess bottom surface area. The three-ring molds with six recesses and the honeycomb molds with one recess were seeded with 8.5×10^5 cells and 7.2×10^5 cells, respectively, corresponding to 50,000 cells per mm^2 of mold recess bottom surface area. The medium was added 20-min post seeding to allow cells to settle. For transforming growth factor (TGF)-β1 experiments, preconfluent cells were pretreated with 5 ng/mL TGF-β1 (Invitrogen) for 48 h before seeding. Media was exchanged every other day.

Microscopy and data analysis

All time lapse microscopy was performed using a Carl Zeiss Axio Observer Z1 equipped with an AxioCam MRm camera and an environmental chamber (37°C, 10% CO_2.). Images were analyzed using ImageJ (Rasband, W.S., NIH) or a combination of Axiovision and Matlab. Cell distributions within dogbone recesses were quantified by analyzing pixel intensities of fluorescent images of CellTracker-stained tissues with ImageJ 3D surface plot. Photobleaching and fluorescence deterioration with time were accounted for by normalizing the total fluorescence of the entire tissue at each time point to the starting fluorescence of the microtissue and adjusting individual pixel intensity measurement values accordingly.

Statistical analysis

Data were analyzed using Stata 11 software (StataCorp, College Station, Texas). For comparison of two means, the Student's t-test was used. For comparison of two proportions, Banard's exact test was used. Kaplan–Meier analysis with the log-rank test was used for comparison of proportion of intact dogbones versus time. Significance was assumed for $p < 0.05$.

Results

We initially focused on molds with the loop-ended dogbone shape because of its relative simplicity with regard to cell-mediated tension. The two posts constrain the microtissue causing tension to form along predominantly one axis, the length of the connecting rod. In this design, it is easy to systemically vary rod length and rod width and determine their effects on stability and point of rupture (Fig. 1 and Supplementary Fig. S1; Supplementary Data are available online at www.liebertpub.com/tea).

NHFs labeled with CellTracker were seeded into agarose molds and imaged using phase-contrast and fluorescent microscopy. ImageJ 3D surface plot was utilized to quantify and confirm uniform cell distribution throughout the dogbone recesses. Time lapse images were also used to follow the morphological changes that occurred as NHFs self-
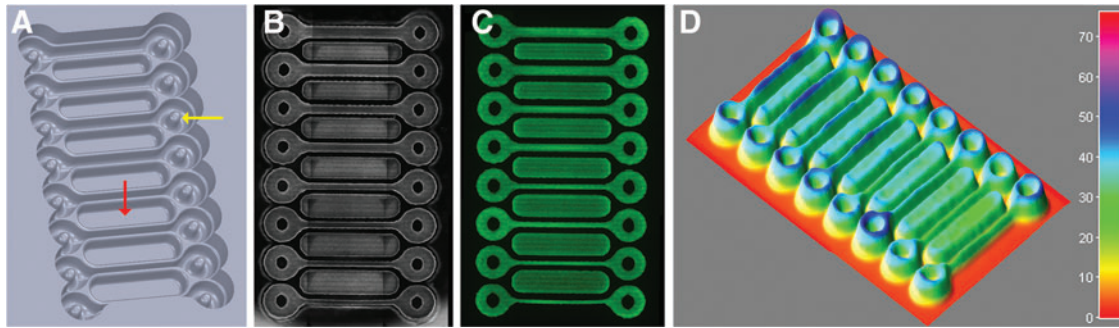
FIG. 1. Micro-mold for creating loop-ended dogbone microtissues. Computer aided design drawing of mold **(A)**. Each dogbone has a toroid around a post (denoted by yellow arrow) at either end joined by a connecting rod (9 mm in length). The width of the connecting rod (from top to bottom, in duplicate) is 800, 600, 400, or 300 μm. The design also includes troughs (red arrow) between the dogbones to eliminate dead space and aid in more uniform cell seeding. Phase-contrast image of normal human fibroblasts (NHFs) settled in dogbone mold immediately after seeding **(B)**. Fluorescent image of NHFs (labeled with CellTracker Green CMFDA) settled in dogbone mold immediately after seeding **(C)**. ImageJ three-dimensional (3D) surface plot of fluorescent image showing uniform cell seeding **(D)**. 24 images (three spanning the length of each of the eight dogbones) were stitched together to make the final images in **B** and **C**. Color images available online at www.liebertpub.com/tea

assembled into the dogbone and exerted tension (Fig. 2 and Supplementary Videos S1–S3). Soon after NHFs were seeded, they aggregated to form a contiguous multicellular dogbone that coalesced around the central posts of the toroid regions and pulled taut the connecting rod portion of the dogbone. Tension in the rod region caused a V-shaped gap to form adjacent to each post. With time, the tension increased around the toroid portions of the tissue, resulting in the closing of the gap, the narrowing and breaking of the tissue in the rod region, and the rapid retraction of the tissue toward the posts.

To examine these morphological changes, we measured the width and fluorescence at different locations over time (Fig. 3). For all plots, tissue width decreased quickly during the first 1.5–2 h marking the initial cell aggregation period. Changes to tissue morphology began after this initial period. At the location of eventual rupture, width and fluorescence remained relatively constant for the next 10 h and then began to decrease exponentially until the tissue ruptured. At locations on either side of the point of rupture, there was little change between 2–10 h followed by a steady decline until the dogbone failed. Interestingly, the V-shaped gap near the posts reached its maximum soon after the initial aggregation period, declined rapidly during the next 10 h, and then slowed until rupture. In contrast to rod width, the decline in the V-shaped gap did not accelerate during the time period immediately before the rupture.

To examine the effect of rod width and length on stability, we formed dogbones with rods of varying width (300, 400, 600, and 800 μm) and varying length (6, 9, and 12 mm) (Fig. 4). The kinetics of rupture showed that as rod width was increased, the time to rupture also increased (i.e., thicker rods were more stable). Dogbones with 800 μm rod widths lasted medians of 36%, 51%, and 79% longer than the dogbones with 600, 400, and 300 μm widths, respectively. In contrast, the time to rupture decreased with increasing length of the rod (i.e., longer rods were less stable). Dogbones with 6 mm rod lengths lasted medians of 26% and 42% longer than the dogbones with 9 and 12 mm rod lengths, respectively. Not all dogbones ruptured. Some dogbones (rod length = 6 mm; rod widths = 600 and 800 μm; initial cell density = 45,000 cells/

mm² of mold surface area) lasted more than 3 days with a very thin connecting rod (data not shown). In addition, dogbones constructed from a different cell type, the H35 hepatocyte cell line (H35), could remain stable for over a week at widths of 600 and 800 μm and all lengths (data not shown). To determine if rod width and length influenced where a dogbone ruptured, we mapped rupture points based on the dogbone's two axes of symmetry. For all rod lengths, and most rod widths, rupture most often occurred in the rod. However, this was not the case for the widest rods (800 μm), which more commonly ruptured in the toroid region.

To study how growth factors might affect stability, we examined the effects of TGF-β1, a known enhancer of fibroblast contractility[20] (Fig. 5). Compared to dogbones formed by untreated cells, TGF-β1-treated dogbones contracted much more rapidly, and the time until rupture was considerably shorter ($p = 0.011$). At 4 h, the rods of TGF-β1-treated dogbones were significantly more narrow than those of untreated dogbones ($p = 0.000003$).

To examine the role of obstacles in a more complex environment, we designed molds to create tissues in the shape of three interconnected toroids aligned in a straight line with either a post (P) or a cone (C) (65° slope) at each of their centers (Fig. 6). All possible post/cone combinations, six in total, were present on each mold. NHFs were seeded onto the molds, and the shape evolutions of the resulting three-ring tissues were followed over time by mapping their edges along a line extending across the centers of the three posts/cones (Fig. 7). The resulting time tracings followed changes to the width and position of the tissue at four points along the tissue. Slight, but distinct, differences were observed for different post/cone combinations. After the initial cell aggregation, the four widths of the three-post (PPP) tissue narrowed, remained narrow over time, and did not shift position. The two outer widths decreased slightly with time, whereas the two inner widths increased slightly with time. In comparison, all four widths of the three-cone (CCC) tissue were significantly wider throughout the entire observation period. In addition, the outer widths of the tissue shifted position inward. The two inner widths initially tapered
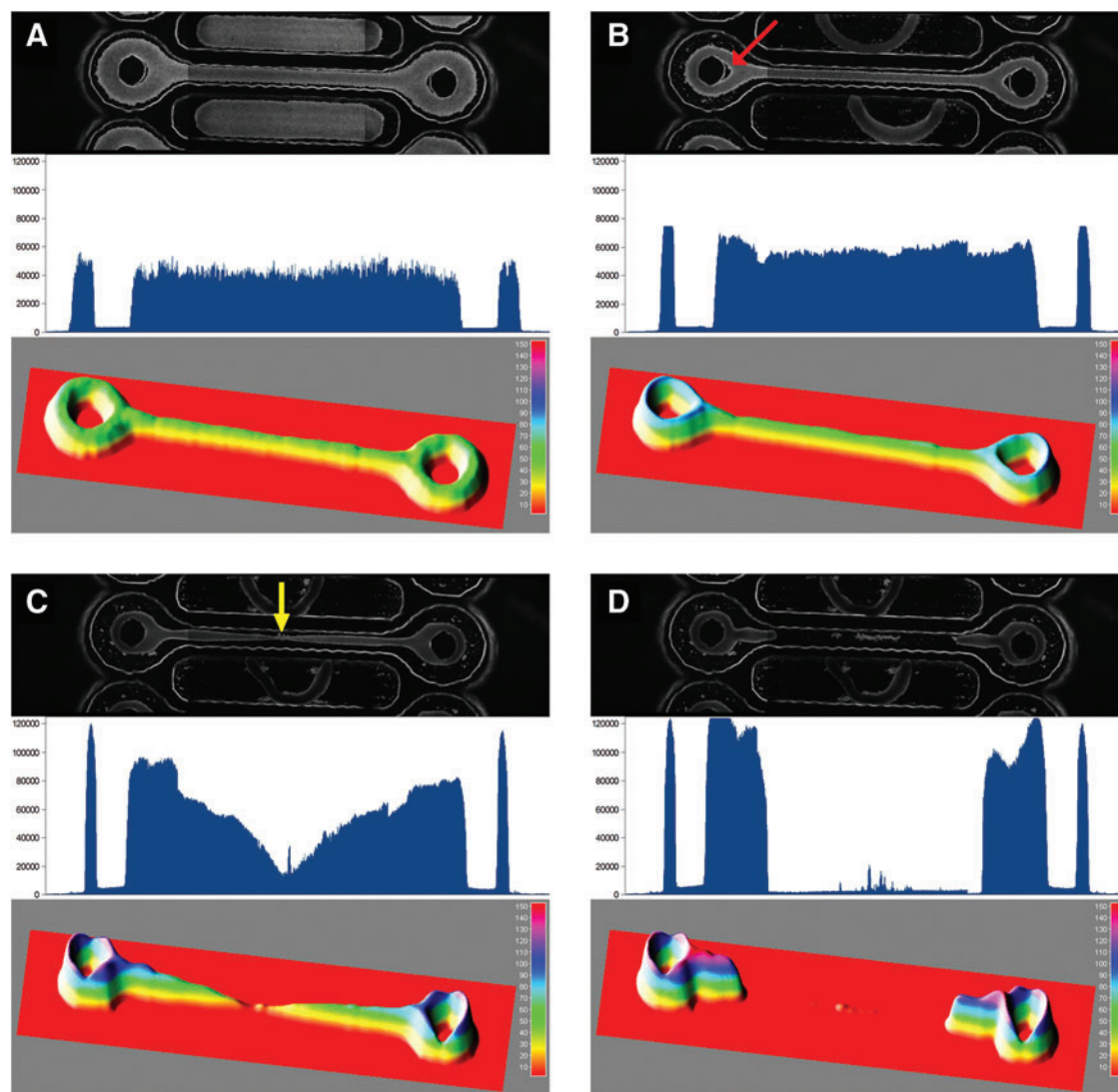
FIG. 2. Multicellular dogbones undergo significant morphological changes after self-assembly. Fluorescent-labeled NHFs were seeded into a mold and self-assembled into a loop-ended dogbone-shaped tissue. The mold design had a connecting rod 9 mm in length and 600 μm in width. Phase-contrast image (top), tracing of fluorescence intensity along line extending across centers of toroids (middle), and 3D surface plot (bottom) of cell distribution at 1 h **(A)**, 2 h **(B)**, 22 h **(C)**, and 22.5 h **(D)**. The red arrow in **(B)** denotes the V-shaped gap that forms between the post and the tissue. The yellow arrow in **(C)** indicates the point of eventual rupture. Three images spanning the length of the dogbone were stitched together to make each final image. Color images available online at www.liebertpub.com/tea

slightly but subsequently widened, whereas the outer widths remained relatively constant. Whenever a cone was present at one of the ends of the tissue, the adjacent outer width of tissue would shift position inward, suggesting that the cone shape allows tension to be released within the tissue.

To examine the influence of cones on larger tissues, we designed two molds for forming honeycomb-shaped tissues (Fig. 8). Each honeycomb had a mix of 19 posts or cones arranged in two orbitals around a single central post/cone. One design had three cones in a row along one side of the outer orbital of the honeycomb. The other design had a single cone in the center and all cones in the outer orbital. In both designs, NHFs aggregated to form honeycomb tissues that exerted tension around the posts/cones. Over time, both designs eventually released their honeycombs. The progres-

sion to release was dependenton the position of the cones. For the design with three cones along one outer edge, release initiated at this edge, whereas for the design with cones around the entire perimeter, release occurred in a circumferential pattern.

Discussion

Using surface molded nonadhesive hydrogels, we have devised a versatile platform for the *in vitro* control of the 3D morphological evolution of self-assembling microtissues. These morphological changes are driven by the cell-mediated forces of self-assembly, including the actions of both surface adhesion molecules and cytoskeletal-mediated contraction,[9,10,12–14] and can be directed by mold design features.
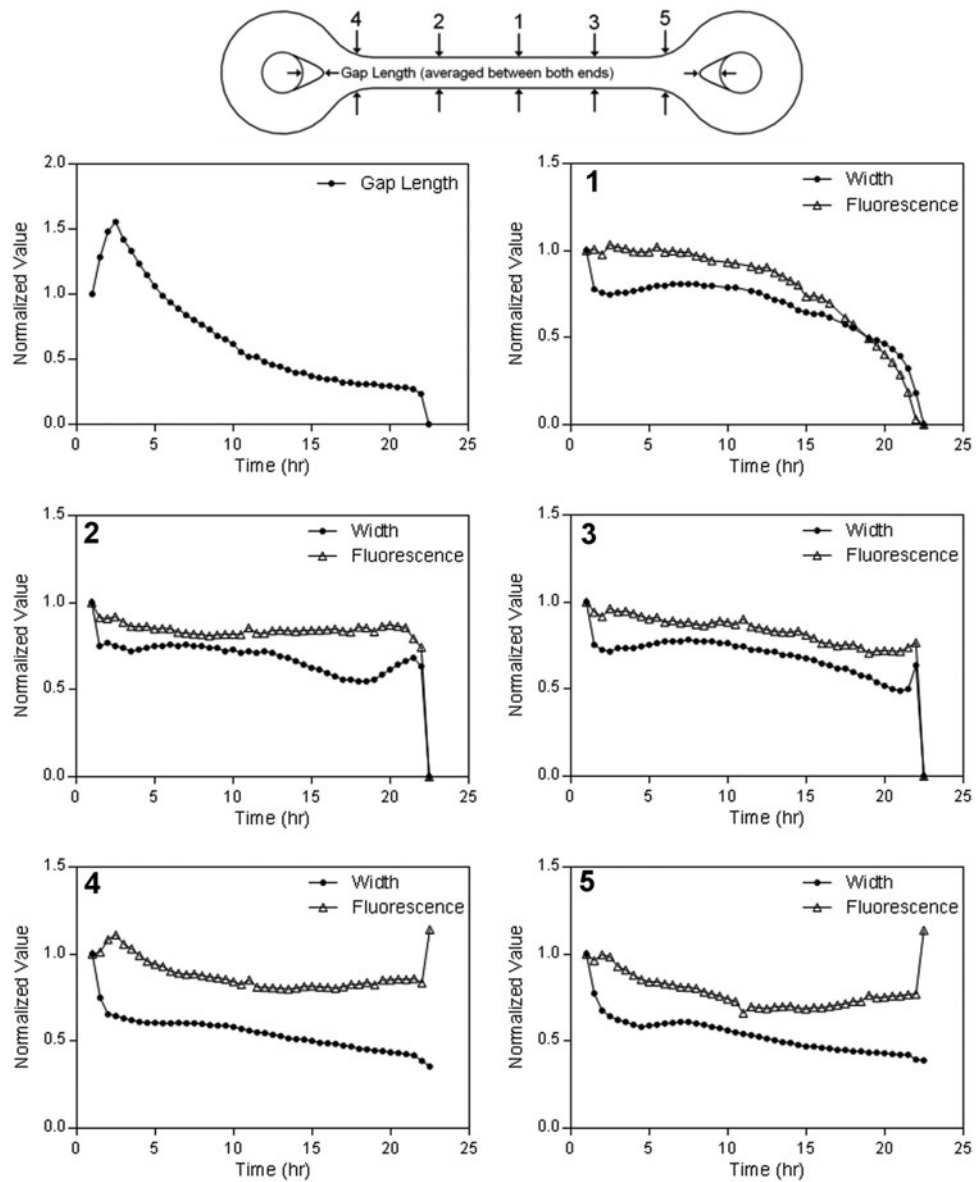
FIG. 3. Rate of morphological change varies at different positions in the dogbone. The change in gap length (upper left) and in width and fluorescence at different locations (denoted by numbers) in a representative loop-ended dogbone (connecting rod 9 mm long, 600 μm wide) were obtained from time lapse fluorescent images. Width measurements were taken from changes in the x, y dimensions of the fluorescent images and gap length was an average of both gaps. All measurements were normalized to their value at the initial time point.

Mold design influences two phases in the process; the phase of cell settling and the phase of cell-driven self-assembly/tissue self-organization. Thus, through mold design, it is possible to control the 3D morphology, provided we understand how tissue self-organization reacts to the various geometries and topographies of different mold features (rules of mold design).

Mold design has two essential features; the size/shape of the mouth of the micro-mold and the topography of the molded hydrogel surface below the mouth. The x, y dimensions of the mouth dictate the footprint into which cells settle and so helps set the initial shape and starting conditions from which self-assembly commences (e.g., dogbone shape). Because cells settle into the mold by gravity, the surface area of the mouth defines how many cells will settle into the mold below. Larger surface areas capture more settling cells. The topography of the molded surface further manipulates the position of the cells as they settle and move past the mouth of the micro-mold. For example, the loop-ended dogbone mold is a recess that has a continuous con-

cave trough. Due to the concavity of the trough, cells settle to the lowest gravitational point along the length of the trough and so are able to uniformly contact neighboring cells. Cell-to-cell contacts initiate self-assembly, so the planar layout of the cells within a dogbone footprint sets the starting point from which subsequent morphological changes ensue.

Another important aspect of the topography of the molded surface is the size, shape, and position of protruding obstacles (Table 1). For example, the dogbone has two vertical obstacles in the shape of posts. These posts serve multiple roles all of which can be easily manipulated via mold design. During the cell settling phase, the posts serve to exclude cells and funnel them down and into the troughs that surround the posts. The diameter of the posts dictates the size of the loops in the dogbone tissue. During self-assembly, the posts have dramatic effects on the morphological evolution of the tissue. The posts are obstacles to self-assembly and they serve as immovable constraints that fix the tissue, thereby creating tension that is sensed by and responded to
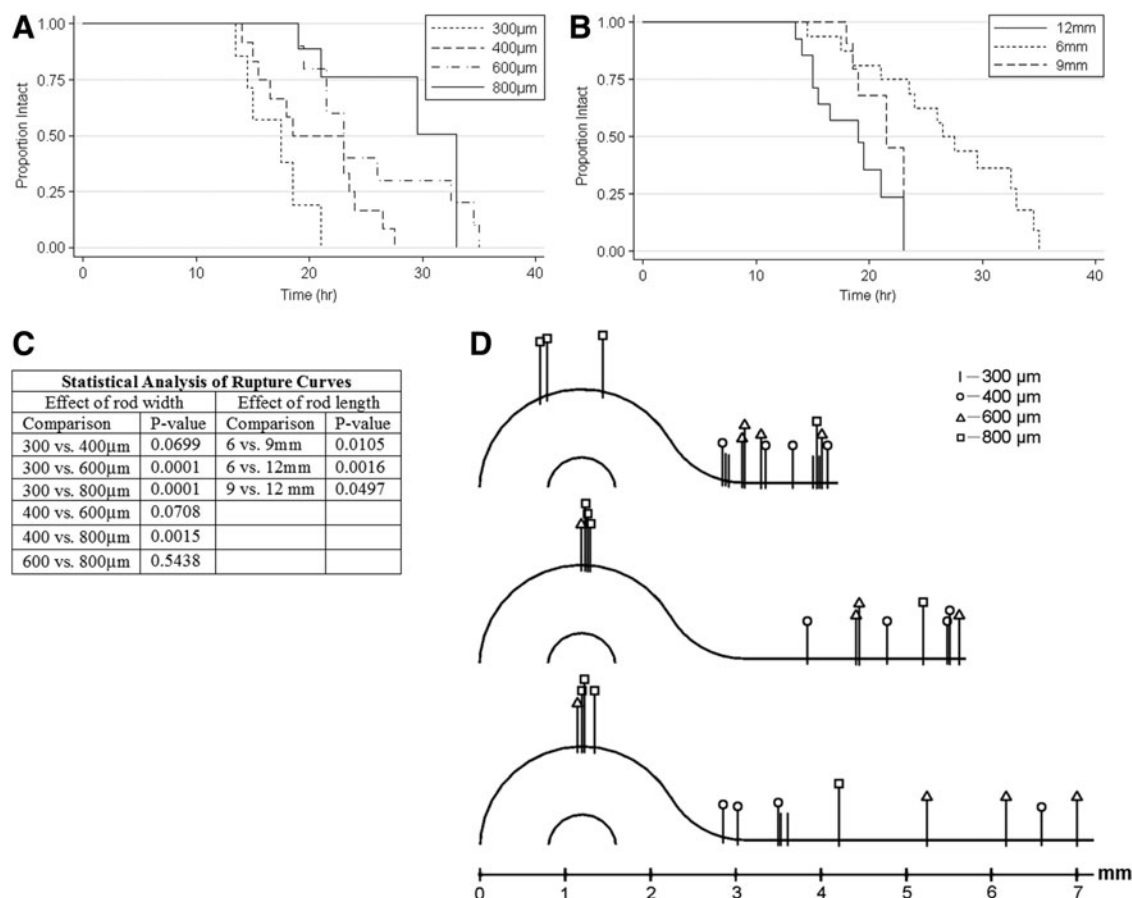
FIG. 4. Connecting rod width and length control the kinetics and location of rupture. Dogbones of varying length (6, 9, 12 mm; $n=16$, 13, 14, respectively) **(A)** and varying width (300, 400, 600, 800 μm; $n=7$, 12, 12, 12, respectively) **(B)** were followed over time, and the proportion of intact dogbones was computed for each time point, resulting in the generation of Kaplan–Meier curves. For these curves, only breaks in the rod region were counted as ruptures; breaks in the toroid regions were censored. Log-rank p-values for pair wise comparisons for the effects of width and length on the rate of rupture were computed **(C)**. The points of rupture of dogbones of varying width were marked to specific locations on maps of dogbones of varying length **(D)**.

by the self-assembling tissue. The position of the posts dictates the lines of tension, which in turn dictates how the tissue self-organizes. For example, the posts of the loop-ended dogbone cause a uniaxial tension to develop that aligns cells, leading to the thinning of the connecting rod and ultimately tissue rupture at a point in between the posts.

Varying the width and length of the connecting rod region showed how these design parameters can control tension in the dogbone tissue. Trough width dictates the cross-sectional area throughout the continuous trough of the dogbone, including the rod and the area surrounding the posts. The larger the cross-sectional area, the more cells there are to resist rupture via cell–cell adhesions and inward radial contractile forces. As rod width was reduced, tissues ruptured sooner because there were fewer cells to resist rupture. Mapping the points of rupture supports this conclusion. When toroid and rod widths were equal, stability was greatest and rupture occurred in both the toroid and rod regions. As rod width was decreased, rupture points shifted preferentially to the rod region.

In contrast, rod length and trough circumference in the toroid region dictate the total number of cells (cell volume)

that exert the uniaxial or circumferential force that eventually causes rupture in the rod or post regions, respectively. The longer the trough, the greater the cell volume; thus, the greater the uniaxial or circumferential force that leads to rupture. Most of our dogbones ruptured even when the trough width was uniform throughout the design, suggesting that the uniaxial and circumferential forces of our most stable design were not perfectly balanced for fibroblasts, a cell type we have shown exerts the greatest forces during self-assembly.[13] After the initial aggregation phase, the most stable dogbone tissue had the following dimensions: uniform tissue width of ~650 μm, rod length of ~3.6 mm, and inner circumference around post of ~2.5 mm. When we increased the length of the rod, we found that longer rods ruptured sooner than shorter rods, presumably because longer rods have a greater cell volume, which exerts greater forces versus the cell volume surrounding the posts. One would expect that rupture should then map preferentially to the toroid region. However, this shift in rupture points was not observed. This may be due to longer rods being more likely to contain a point of nonuniformity that would act as a nidus for rupture.
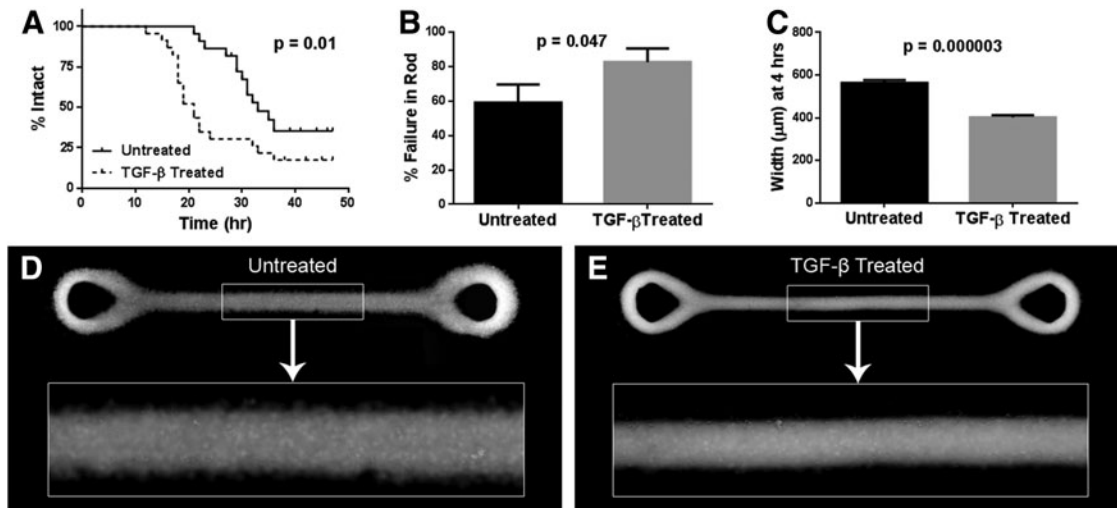
FIG. 5. Transforming growth factor (TGF)-β1 treatment decreases the time to rupture and increases the rate of microtissue contraction. Kaplan–Meier curves following dogbones composed of TGF-β1-treated NHFs ($n=23$) and untreated NHFs ($n=22$) until rupture in the rod region show that TGF-β1 treatment significantly reduces the time until rupture ($p=0.011$) **(A)**. For these curves, only breaks in the rod region were counted as ruptures; breaks in the toroid regions were censored. TGF-β1 treatment increased the percentage of breaks in the rod region ($p=0.047$) **(B)**. TGF-β1 treatment led to significantly decreased rod width at 4 h ($p=0.000003$) for dogbones with an initial rod width of 800 μm ($n=5$) **(C)**. Error bars represent standard errors. Also shown are representative fluorescent images of an untreated **(D)** and a TGF-β1-treated **(E)** dogbone (labeled with CellTracker Green) at the 4-h time point. Three images spanning the length of the dogbone were stitched together to make each final image.
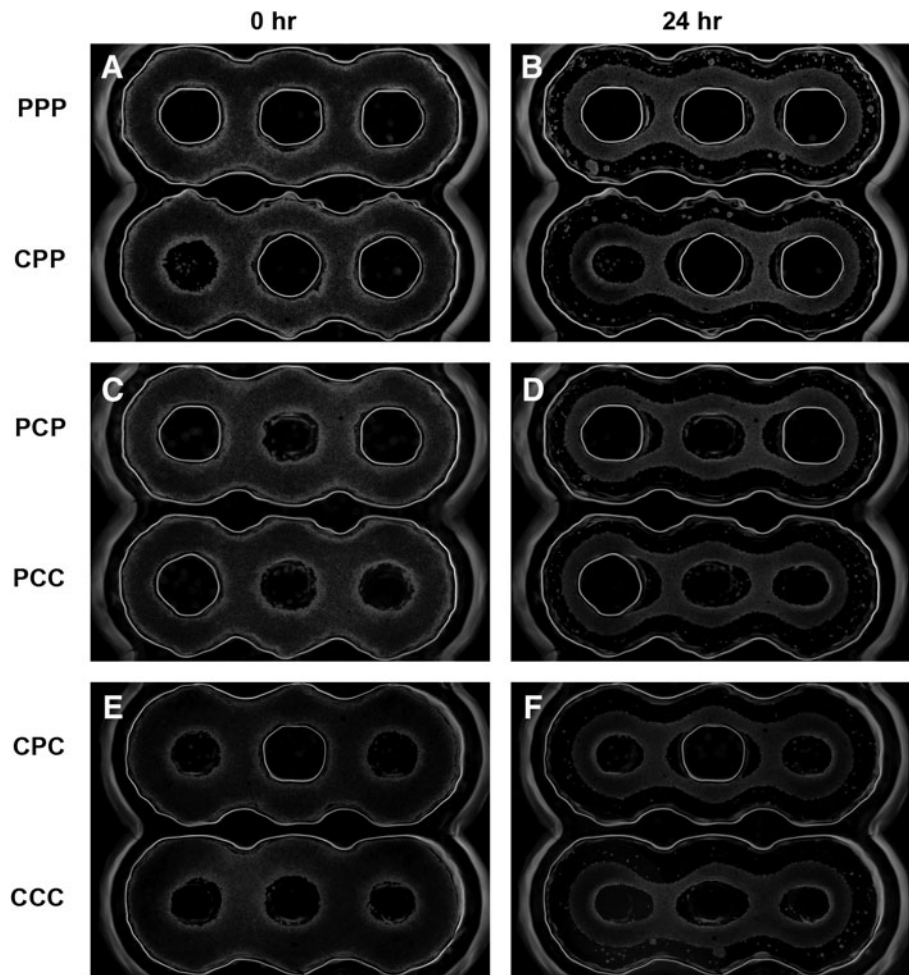
FIG. 6. Obstacle shape and position control the evolution of microtissue morphology. Three-ring microtissues were formed in a series of different molds. Each mold had three obstacles, each in the form of either a post (P) or a cone (C). The left to right order of the obstacles is labeled in the left margin. Molds were seeded with NHFs, and time lapse phase-contrast images taken at time zero when the cells had settled **(A, C, E)** and 24 h later **(B, D, F)** are shown. Scale bar is 500 μm.
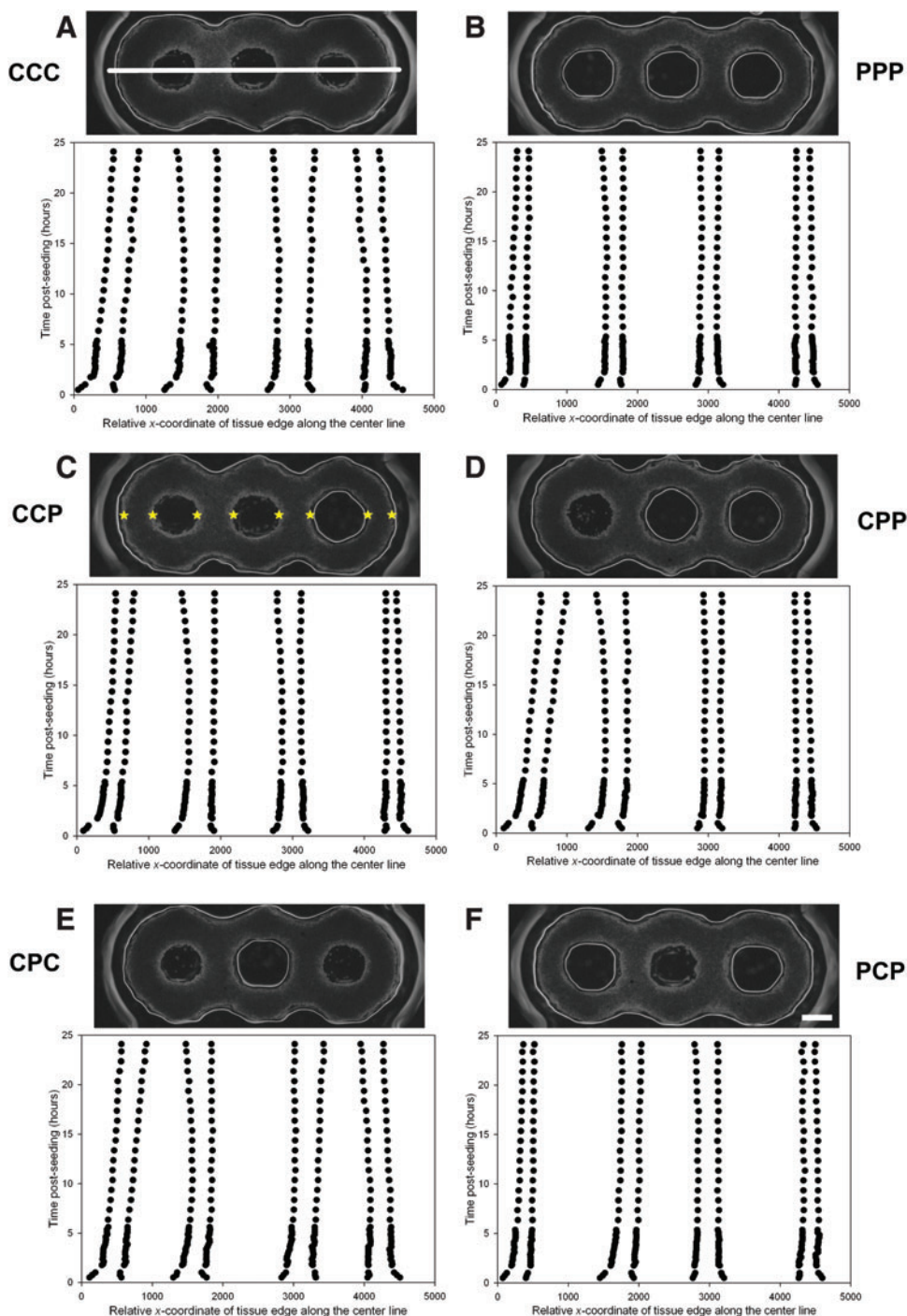
FIG. 7. Morphological changes to three-ring microtissues as a function of time, obstacle shape, and position. Three-ring microtissues were formed in a series of molds with three obstacles, each in the shape of a post (P) or a cone (C). The left to right order of the obstacles is labeled. Change in tissue shape over time was quantified from time lapse images by mapping the edges (width) of the tissues along a line connecting the centers of the three obstacles. The white line shown in **(A)** is the center line. The stars in **(C)** indicate the edges of the tissue which were mapped. Scale bar in **(F)** is 500 μm. Color images available online at www .liebertpub.com/tea

Points of rupture are of interest to morphological analyses because they are locations of greatest tension that dramatically alter both the tissue as well as the cells in that location. Cells can react to this high-tension environment in several interesting ways at both the cellular (e.g., stretching) and molecular levels. It would be interesting to investigate the nature and organization of the focal adhesions at these sites of high tension and cell stretching.

Tension can be modulated by the design of the shape of an obstacle dictating when and where tension is released in a self-organizing tissue. Posts with vertical sides create the highest level of tension in a tissue and sustain this tension for

the longest time. In the dogbone, this sustained tension results in an eventual tissue rupture. In contrast, an obstacle in the shape of a cone creates tension, but this tension is gradually released as the tissue slides up the nonadhesive cone, a tension modulator. Previously, we showed that toroid-shaped tissues of the H35 hepatocyte cell line were sensitive to a cone's slope, with toroids moving more slowly up a steep slope (85°) than a shallow slope (55°).[13] In contrast, the rate of movement of NHF toroids was unaffected by slope. Thus, the rate at which tension in a tissue is released is related to the cell type and the slope of the cone. The time over which this tension is completely released is related
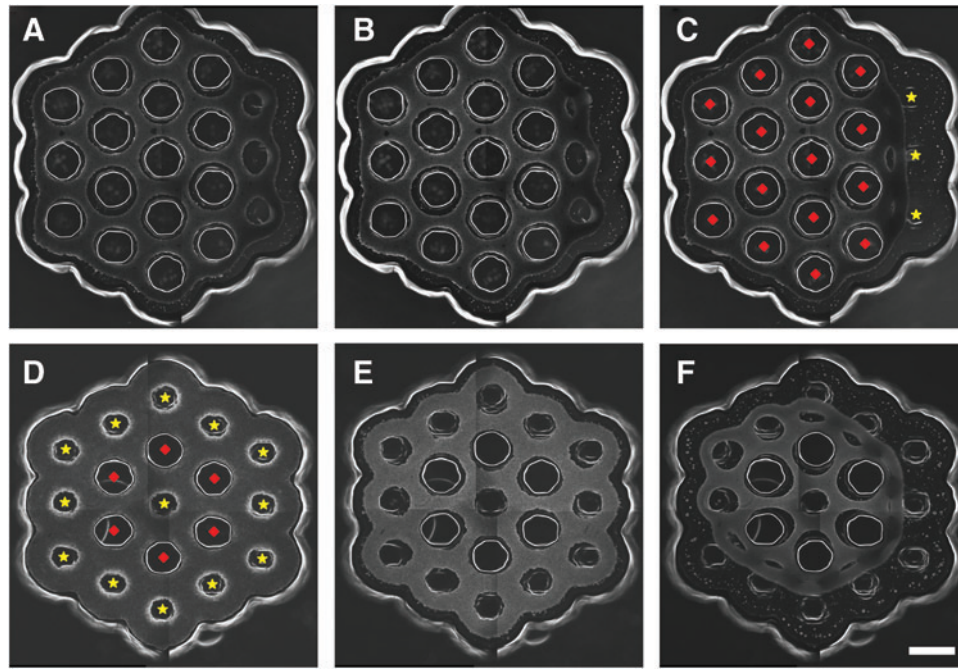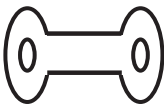
FIG. 8. Obstacle position and shape control release of honeycomb microtissues. Molds designed to form a large honeycomb tissue were seeded with NHFs, and phase-contrast images were taken to document the obstacle-mediated morphological changes that result in the release of the honeycomb from the mold. One honeycomb design had three cones in a row along one outer edge of the honeycomb. Images at 34 h **(A)**, 40 h **(B)**, and 46 h **(C)** after seeding show that honeycomb release starts at the edge containing the three cones. Another honeycomb design had a single cone in the center and 12 cones around the outer edge. Images at time zero **(D)**, 4 h **(E)**, and 24 h **(F)** after seeding show that honeycomb release occurs in a circumferential pattern. The diamonds and stars in **(C)** and **(D)** indicate posts and cones, respectively. Scale bar is 1000 μm. Color images available online at www.liebertpub.com/tea

to the height of the cone. Furthermore, as shown with three-ring tissues and honeycomb tissues, the placement of cones versus posts in a design dictates where tension is released in a large self-organizing tissue.

Our measurements of morphological changes in the dog-bones revealed three phases in tissue self-organization. The first phase commenced soon after the cells had settled and conformed to the bottom of the mold and formed the initial cell-to-cell connections. Over the next 3 h, cells rapidly aggregated as shown by the rapid reduction in width at all locations along the dogbone. Fluorescence, a measure of cell density at these locations, was relatively unchanged indicating that the decrease in width (x, y) gave rise to a corresponding increase in the height (z) of the tissue. During this

TABLE 1. ELEMENTS OF MOLD DESIGN THAT INFLUENCE MORPHOLOGICAL EVOLUTION

Schematic of design elements	Design feature	How design element controls morphological evolution
	Rod length	Shorter rods more stable, predictable time to rupture, predictable point of rupture, rupture point dependent on width, no rupture for some cell types
	Rod width	Wider rods more stable, predictable time to rupture, influences point of rupture, no rupture for some cell types (e.g., H35)
	Post diameter	Creates circumferential tension around post, creates uniaxial tension between two posts, controls diameter of microtissue
	Post height	Minimum height needed for stability
	Cone diameter	Dictates starting point of circumferential tension
	Cone height	Dictates time until tissue is released from mold
	Cone slope	Dictates rate at which tension is dissipated
	Placement of obstacles	Controls overall size and shape of microtissue, dictates lines of tension in microtissue, controls when and where tension is released

time, the loose aggregate of cells (cell adhesions mostly in the x, y planes) that had initially conformed to the bottom of the mold moved to a state where they were a super aggregate (cell adhesions in all planes) that had lifted from the mold floor and conformed to the posts.[21] During this time, tension increased in the tissue as evidenced by the rapid increase in the length of the V-shaped gap near both posts. In the second phase over the next 10 h, the gap decreased rapidly and then slowed. The decrease in the V-shaped gap does not indicate that tension is decreasing in the dogbone. Rather, it shows that tension is redistributing from the initial global tension of the super-aggregate to a uniaxial direction that will ulti-mately lead to the rupture. During these 10 h, there was little change in width or fluorescence at all locations along the connecting rod even at the point of eventual rupture. In the third and final phase over the next 10 h, the decrease in the V-shaped gap slowed considerably and all points along the rod region remained unchanged or underwent a slow decrease, except for the point of eventual rupture. At this point, both width and fluorescence declined slowly at first, but this decline accelerated as rupture approached. The de-crease in width and fluorescence indicate that cellular material was being lost from this point possibly by cell movement, breaking of cell-to-cell connections, and cell stretching. Clearly, cell-to-cell connections are broken because the tissue eventually ruptures, but we have also observed cell stretch-ing. Previously, we showed that fibroblasts could stretch up to 30 times their initial cell diameter.[21] It would be interesting to determine the relative contributions of stretching, move-ment, and bond breaking to the thinning of the tissue.

Cell types differ significantly with regard to their rate and extent of self-assembly.[13,15] Of the cell types tested, fibro-blasts exert the greatest forces, which is why dogbone tissues often rupture. Other cell types, such as H35s, self-assemble tissues that are stable but are also under tension. Using a toroid-on-a-cone assay, we have shown that fibroblasts exert ~ 10 times more cell power than H35s during self-assembly, and, when mixed with H35s, fibroblasts exert even more power per cell.[22] Although we are just beginning to under-stand how cell types react to different features of mold design, fibroblasts are especially informative because they self-assemble rapidly and create and respond to tension and can hence quickly reveal tissue reactions to new mold designs.

We have demonstrated that micro-mold design controls the morphological evolution of self-organizing tissues con-stituted from individual cells. In addition to controlling tis-sue shape, design elements can control the tension that develops, thereby causing the tissue to undergo prescribed morphological changes. There are countless possibilities in mold design and we are just beginning to understand how self-organizing tissues react to the geometry of selected fea-tures and how we can use these features to control tissue organization. This knowledge is useful for complex mold designs for numerous applications. Self-organizing tissues with controlled tension are useful testbeds to evaluate growth factors on 3D cell mechanics such as TGF-β1 or drugs that target the cellular machinery driving cell–cell tension.[22] Of note, cell tension is thought to underlie pathological states, such as fibrosis.[23] Likewise, during the develop-ment, cell-mediated tension drives and influences organ morphogenesis.[24] Mold design can be used to produce more accessible *in vitro* models that recapitulate complex devel-opmental processes. Finally, mold design may prove useful to the use of self-assembled tissues as building blocks for larger tissues.[25,26] In addition to controlling the shape of a building block, tension can control the timing and location of the release of a building block from its mold.

Disclosure Statement

J.R.M. has an equity interest in Microtissues, Inc. This re-lationship has been reviewed and managed by the Brown University in accordance with its conflict of interest policies.

References

1. Moscona, A., and Moscona, H. The dissociation and aggre-gation of cells from organ rudiments of the early chick em-bryo. J Anat **86,** 287, 1952.
2. Kelm, J.M., and Fussenegger, M. Microscale tissue engi-neering using gravity-enforced cell assembly. Trends Bio-technol **22,** 195, 2004.
3. Kelm, J.M., Ittner, L.M., Born, W., Djonov, V., and Fusse-negger, M. Self-assembly of sensory neurons into ganglia-like microtissues. J Biotechnol **121,** 86, 2006.
4. Kunz-Schughart, L.A., Schroeder, J.A., Wondrak, M., van Rey, F., Lehle, K., Hofstaedter, F., *et al.* Potential of fibro-blasts to regulate the formation of three-dimensional vessel-like structures from endothelial cells *in vitro*. Am J Physiol Cell Physiol **290,** C1385, 2006.
5. Fukuda, J., and Nakazawa, K. Orderly arrangement of he-patocyte spheroids on a microfabricated chip. Tissue Eng **11,** 1254, 2005.
6. Ofek, G., Revell, C.M., Hu, J.C., Allison, D.D., Grande-Allen, K.J., and Athanasiou, K.A. Matrix development in self-assembly of articular cartilage. PloS One **3,** e2795, 2008.
7. Desroches, B.R., Zhang, P., Choi, B.R., King, M.E., Mal-donado, A.E., Li, W., *et al.* Functional scaffold-free 3-D car-diac microtissues: a novel model for the investigation of heart cells. Am J Physiol Heart Circ Physiol **302,** H2031, 2012.
8. Gwyther, T.A., Hu, J.Z., Christakis, A.G., Skorinko, J.K., Shaw, S.M., Billiar, K.L., *et al.* Engineered vascular tissue fabricated from aggregated smooth muscle cells. Cells Tis-sues Organs **194,** 13, 2011.
9. Dean, D.M., and Morgan, J.R. Cytoskeletal-mediated tension modulates the directed self-assembly of microtissues. Tissue Eng Part A **14,** 1989, 2008.
10. Krieg, M., Arboleda-Estudillo, Y., Puech, P.H., Kafer, J., Graner, F., Muller, D.J., *et al.* Tensile forces govern germ-layer organization in zebrafish. Nat Cell Biol **10,** 429, 2008.
11. Foty, R.A., Pfleger, C.M., Forgacs, G., and Steinberg, M.S. Surface tensions of embryonic tissues predict their mutual envelopment behavior. Development **122,** 1611, 1996.
12. Foty, R.A., and Steinberg, M.S. Cadherin-mediated cell-cell adhesion and tissue segregation in relation to malignancy. Int J Dev Biol **48,** 397, 2004.
13. Youssef, J., Nurse, A.K., Freund, L.B., and Morgan, J.R. Quantification of the forces driving self-assembly of three-dimensional microtissues. Proc Natl Acad Sci U S A **108,** 6993, 2011.

14. Bao, B., Jiang, J., Yanase, T., Nishi, Y., and Morgan, J.R. Connexon-mediated cell adhesion drives microtissue self-assembly. Faseb J **25,** 255, 2011.

15. Dean, D.M., Napolitano, A.P., Youssef, J., and Morgan, J.R. Rods, tori, and honeycombs: the directed self-assembly of microtissues with prescribed microscale geometries. Faseb J **21,** 4005, 2007.

16. Achilli, T.M., McCalla, S., Tripathi, A., and Morgan, J.R. Quantification of the kinetics and extent of self-sorting in three dimensional spheroids. Tissue Eng Part C Methods **18,** 302, 2012.

17. Napolitano, A.P., Chai, P., Dean, D.M., and Morgan, J.R. Dynamics of the self-assembly of complex cellular aggregates on micromolded nonadhesive hydrogels. Tissue Eng **13,** 2087, 2007.

18. Napolitano, A.P., Dean, D.M., Man, A.J., Youssef, J., Ho, D.N., Rago, A.P., *et al.* Scaffold-free three-dimensional cell culture utilizing micromolded nonadhesive hydrogels. Biotechniques **43,** 494, 496, 2007.

19. Tejavibulya, N., Youssef, J., Bao, B., Ferruccio, T.M., and Morgan, J.R. Directed self-assembly of large scaffold-free multi-cellular honeycomb structures. Biofabrication **3,** 034110, 2011.

20. Liu, X.D., Umino, T., Ertl, R., Veys, T., Skold, C.M., Takigawa, K., *et al.* Persistence of TGF-beta1 induction of increased fibroblast contractility. *In vitro* Cell Dev Biol Animal **37,** 193, 2001.

21. Dean, D.M., Rago, A.P., and Morgan, J.R. Fibroblast elongation and dendritic extensions in constrained versus un-constrained microtissues. Cell Motil Cytoskeleton **66,** 129, 2009.

22. Youssef, J., Chen, P., Shenoy, V.B., and Morgan, J.R. Mechanotransduction is enhanced by the synergistic action of heterotypic cell interactions and TGF-beta1. Faseb J **26,** 2522, 2012.

23. Gabbiani, G. The myofibroblast in wound healing and fibrocontractive diseases. J Pathol **200,** 500, 2003.

24. Mammoto, T., and Ingber, D.E. Mechanical control of tissue and organ development. Development **137,** 1407, 2010.

25. Mironov, V., Visconti, R.P., Kasyanov, V., Forgacs, G., Drake, C.J., and Markwald, R.R. Organ printing: tissue spheroids as building blocks. Biomaterials **30,** 2164, 2009.

26. Rago, A.P., Dean, D.M., and Morgan, J.R. Controlling cell position in complex heterotypic 3D microtissues by tissue fusion. Biotechnol Bioeng **102,** 1231, 2009.

Address correspondence to:
Jeffrey R. Morgan, PhD
Center for Biomedical Engineering
Brown University
G-B 393, Biomed Center
171 Meeting Street
Providence, RI 02912

E-mail: jeffrey_morgan@brown.edu